

Modeling and Analysis of VOC-based Interplant Molecular Communication Channel

Bitop Maitra[✉], *Graduate Student Member, IEEE* and Ozgur B. Akan[✉], *Fellow, IEEE*

Abstract—Molecular communication (MC) enables information transfer using particles inspired by biological systems. Volatile Organic Compounds (VOCs) are one of the most abundant and diverse classes of signaling molecules used by living or non-living objects. VOC-based MC holds great promise in developing long-range, bio-compatible communication systems capable of interfacing nano- and micro-scale devices. In this paper, we present a comprehensive end-to-end framework for VOC-based interplant MC from an ICT perspective. The communication process is divided into three stages: transmission (VOC biosynthesis and emission from leaves), channel propagation (advection-diffusion in turbulent wind via Gaussian puff for stress-induced VOC release and Gaussian plume for constitutive VOC release), and reception (VOC uptake and physiological response in the receiver plant). Each stage is analyzed by its attenuation and delay. Numerical results demonstrate that VOC-based channels exhibit low-pass behavior, with bandwidth and capacity heavily influenced by distance, wind velocity, and noise. Though the physical channel supports moderate frequencies, biological constraints at the transmitter restrict the end-to-end channel to slow-varying signals.

Index Terms—Molecular Communication, Volatile Organic Compounds (VOC), Plant Communication, Stress-driven VOC Emission, Constitutive VOC Emission, Channel Modeling.

I. INTRODUCTION

MOLECULAR Communication (MC) is an emerging communication paradigm that considers molecular motion as a propagating mechanism aiming to study biological and chemical communication systems by mimicking them as communication networks and studied through Information and Communication Technology (ICT) [1]. Similar to the wireless communication, MC also comprises of a transmitter, a channel, and a receiver, where Information Molecules (IM) are used as the information carrier [2]. However, IMs vary depending on the type of biological or chemical environment; some widely explored IMs are proteins like nucleic acids, ions, chemical messengers, nanoparticles. For plants, these IMs are pheromones, typically Volatile Organic Compounds (VOCs) [3].

VOCs are low-molecular-weight chemicals that are emitted into the atmosphere by plants as part of their physiological functions. Plants have developed the ability to produce and emit different VOCs due to the internal or external biotic and abiotic factors that represent the physiological status

The authors are with the Center for neXt-generation Communications (CXC), Department of Electrical and Electronics Engineering, Koç University, Istanbul 34450, Turkey (e-mail: {bmaitra23, akan}@ku.edu.tr).

O. B. Akan is also with the Internet of Everything (IoE) Group, Electrical Engineering Division, Department of Engineering, University of Cambridge, Cambridge CB3 0FA, UK (email: oba21@cam.ac.uk).

This work was supported by the AXA Research Fund (AXA Chair for Internet of Everything at Koç University).

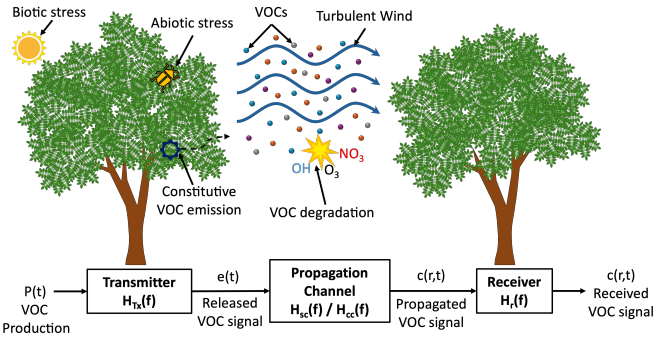


Fig. 1: Schematic diagram of VOC-based end-to-end interplant communication.

of the plant [4]. VOCs are used for mating purposes and potentially repelling any predators while attracting mutualists such as beneficial microbes [5]. The release of VOCs is of two types, namely constitutive and stress-driven [6]. Studies have shown that VOCs play crucial roles in plant-environment and interplant communication under biotic or abiotic stress. Stress-driven emissions are often induced and can vary depending on environmental conditions and the nature of the stress [7]. It is evident that the constitutively emitted VOCs are released continuously [8], whereas stress-driven VOCs are released almost instantly when abiotic and biotic stress are experienced and act as an immediate alarm signal [9]. Based on VOCs, neighboring plants communicate, as shown in Fig. 1, and the receiver plant can either infer the identity of the emitter plant or VOCs can be used to enhance the resistance systems against harmful interactions with herbivorous insects and environmental conditions, such as drought or mechanical injury [10].

Usually, the impact of individual VOCs like methyl jasmonate or isoprene is studied on receiver plants [11]. However, studies show that plants release complex mixtures of VOCs, known as blended VOCs. These blends can carry more detailed information than individual VOCs due to the diversity in their composition and relative ratios [12]. Blended VOCs have been shown to enhance the reliability of the signal received by neighboring plants. For example, receiver plants may respond differently to the same VOC depending on the concentration of different compounds in the blend [13]. This emphasizes the importance of studying VOCs as blends.

Primarily, MC-based communication channels are of limited range, typically in millimeters and investigate the communication either in nanoscale devices or in cellular environments. However, VOC-based MC communication occurs at the unicellular level, like bacteria [14], as well as the multicellular

level, like animals [15]. This channel exists in the surroundings that can range up to hundreds of meters [16]. With the potential of long-range communication along with the existence inside all types of living organisms, it paves a way to connect the microscale environment to the macro-world. Hence, the application of VOC-based communication is large, such as plant communication, plant bird communication [17], stale food or body part and their attractor, pest control, etc. An understanding of the VOC communication channel is required to understand how those species can actually infer the VOC signals.

In environments, interplant VOC propagation occurs through the ambient air, which acts as the physical communication channel. VOCs released from plant surfaces diffuse passively under still air conditions, governed by Fick's laws; however, their transmission is dominated by wind-driven advection and turbulent mixing [18]. Environmental factors like oxidant sources (e.g., hydroxyl radical (OH), nitrate radical (NO_3), ozone (O_3)) also modulate VOCs lifetime and transport range [19]. These atmospheric variables influence the concentration, delay, and directionality of VOC transmission.

VOC-based communication systems from the ICT perspective have not been widely explored. However, a simple channel is described without considering the uncertainties or propagation noise in [20]. Moreover, an end-to-end VOC propagation channel is modeled in [16]. This model considers the advection and turbulent diffusion and obtains the channel attenuation and channel delay for the instantaneous release of a single VOC (linalool). However, it lacks considering noise that is induced by the VOC degradation with the interaction with environmental radicals, and it also doesn't consider the blended VOC release from the transmitter. Hence, a comprehensive study is needed to understand how the channel behaves in real environmental conditions for the stress-driven and constitutive release of VOCs.

In this paper, we consider plants as VOC transmitters and receivers, as shown in Fig. 1. The emission of VOCs may occur via leaves, canopy, and stems; however, the emission from leaves are well documented, and high amounts of VOCs are released from leaves. Hence, we consider the leaf-level emission of VOCs from the stomata of a single leaf [21]. The released VOCs then travel through the ambient air media and the receiver plant uptakes the VOCs into the intercellular airspace through the stomata. Upon diffusing into a leaf, the plant activates the physiological responses according to the detected VOCs. The different steps of VOC communication, i.e., transmission, physical communication channel, and reception, are modeled and analyzed with the normalized gain and the delay.

The rest of the paper is as follows. Sec. II describes the transmission process after the production of VOCs and the release mechanism from the stomata. In Sec. III, the physical channel is modeled considering the stress-driven and constitutive release of VOCs along with a noise model. Then, the reception process or the uptake process of the receptor plant's leaf is described in Sec. IV. Furthermore, Sec. V discusses the numerical results for channel attenuation and delay with physical explanations. It also briefly describes the

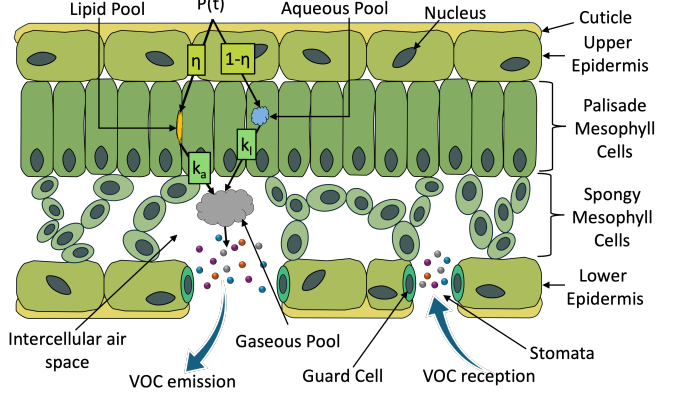


Fig. 2: Schematic diagram of leaf cross-section showing VOC production, emission, and reception through stomata [21], [23].

end-to-end VOC channel model. Finally, Sec. VI concludes this paper with a future direction of VOC-based molecular communication.

II. VOC PRODUCTION AND TRANSMISSION MODEL

In this study, we consider that the VOCs are released from the leaves of a plant. A leaf consists of an upper and lower epidermis, each usually one cell thick and covered by a waterproof cuticle made of cutin to minimize water loss. Beneath the upper epidermis lies the palisade mesophyll comprising elongated chloroplast-rich cells. The spongy mesophyll, made up of loosely packed and spherical cells with large intercellular air spaces that facilitate gas exchange, is found underneath. Stomata, consisting of a pore guarded by two guard cells, regulate the exchange of VOCs, as shown in Fig. 2.

Specialized secretory cells and structures, like trichomes, idioblasts, cavities, and secretory ducts, are responsible for the synthesis of VOCs in plants, such as terpenes and essential oils. These compounds are synthesized in various subcellular compartments, mainly in plastids, often leucoplasts devoid of ribosomes and thylakoids for monoterpenes, and sometimes in mitochondria and Endoplasmic Reticulum (ER). In some species, mitochondria have been directly involved in VOC synthesis. Periplastidic ER surrounds the plastids and may function as a transport duct for the synthesized VOCs. The ER and sometimes Golgi-derived vesicles mediate the intracellular trafficking of VOCs toward the plasma membrane. Once transported, the VOCs are secreted through two main mechanisms: eccrine secretion, i.e., direct molecular or ionic transport across membranes, and granulocrine secretion, i.e., via fusion of vesicles with the plasma membrane. Finally, depending on the structure of the secretory tissue, the VOCs accumulate in subcuticular spaces or are released through pores in the cuticle. The secretory cells are supported by stalk cells with completely cutinized side walls, which prevent the backflow of accumulated VOCs into the plant [22].

After the production of VOCs, i.e., $P(t)$, they are partitioned according to their solubility, as shown in Fig. 2. If the VOCs are water soluble, they are stored in aqueous pools (S_a). The

rate of release of the VOCs from the aqueous pools can be described by the first-order kinetics equation as [21]:

$$\frac{dS_a(t)}{dt} = \eta P(t) - k_a S_a(t), \quad (1)$$

where k_a is the aqueous storage pool VOC-specific first-order kinetic constant, and η is the partitioning coefficient that depends on the solubility and the diffusion coefficient of the VOCs. On the other hand, if VOCs are lipid soluble, they are stored in lipid pools (S_l). The release rate of these lipid soluble VOCs can be expressed as:

$$\frac{dS_l(t)}{dt} = (1 - \eta) P(t) - k_l S_l(t), \quad (2)$$

where k_l is lipid storage pool VOC specific first-order kinetic constant. The VOCs of these pools then diffuse to the intercellular air space of the leaf before the emission to the ambient air medium. The released VOCs are stored in the gas phase pools, known as S_g . From the gas phase pools, the release rate of VOCs to the ambient air can be expressed as:

$$\frac{dS_g(t)}{dt} = k_a S_a(t) + k_l S_l(t) - k_g S_g(t), \quad (3)$$

where k_g depends on the stomatal conductance between intercellular air space and the ambient air, along with the gas phase conductance from the outer cell surface wall to the intercellular air space. It is the flux of VOCs that are released from the leaf gas phase pool into the ambient air. The VOC emission rate ($e(t)$) from the leaf can be expressed as:

$$e(t) = k_g S_g(t), \quad (4)$$

The Fourier transform of the pheromone emission rate is given by:

$$E(f) = k_g S_g(f), \quad (5)$$

From (1-5), we can deduce the transfer function as:

$$H_{Tx}(f) = \frac{k_g}{j2\pi f + k_g} \times \left(\frac{k_a \eta}{j2\pi f + k_a} + \frac{k_l (1 - \eta)}{j2\pi f + k_l} \right), \quad (6)$$

The transfer function, $H_{Tx}(f)$, depends on the solubility coefficient η . However, we are interested in determining the normalized gain as it shows how the signal is attenuated during the diffusion from the intercellular air space to the ambient air. The normalized gain of the transmission can be expressed as:

$$H_{Tx}^n(f) = \frac{k_g}{\sqrt{k_g^2 + (2\pi f)^2}} \sqrt{Im^2(f) + Re^2(f)}, \quad (7)$$

where

$$Im(f) = \left(\frac{k_a \eta \cdot 2\pi f}{k_a^2 + (2\pi f)^2} + \frac{k_l (1 - \eta) \cdot 2\pi f}{k_l^2 + (2\pi f)^2} \right), \quad (8)$$

$$Re(f) = \left(\frac{k_a^2 \eta}{k_a^2 + (2\pi f)^2} + \frac{k_l^2 (1 - \eta)}{k_l^2 + (2\pi f)^2} \right), \quad (9)$$

Moreover, the phase of $H_{Tx}(f)$ is expressed as:

$$\begin{aligned} \phi_{Tx}(f) &= \tan^{-1} \left(\frac{Im(H_{Tx}(f))}{Re(H_{Tx}(f))} \right), \\ &= \tan^{-1} \left(-\frac{2\pi f}{k_g} \right) + \tan^{-1} \left(-\frac{Im(f)}{Re(f)} \right), \end{aligned} \quad (10)$$

Hence, the delay, which captures the arrival time of the VOC signal considering the diffusion, can be obtained as:

$$\begin{aligned} \tau_{Tx}(f) &= -\frac{d\phi_{Tx}(f)}{df} = \frac{2\pi k_g}{k_g^2 + (2\pi f)^2} + \\ &\quad \frac{Re(f) \cdot Im'(f) - Im(f) \cdot Re'(f)}{Re^2(f) + Im^2(f)}, \end{aligned} \quad (11)$$

where $Re'(f)$ and $Im'(f)$ are the first order derivative of $Re(f)$ and $Im(f)$, and given by:

$$Re'(f) = -\frac{8\pi^2 k_a^2 \eta f}{(k_a^2 + (2\pi f)^2)^2} - \frac{8\pi^2 k_l^2 (1 - \eta) f}{(k_l^2 + (2\pi f)^2)^2}, \quad (12)$$

$$\begin{aligned} Im'(f) &= \frac{2\pi k_a \eta (k_a^2 - (2\pi f)^2)}{(k_a^2 + (2\pi f)^2)^2} + \\ &\quad \frac{2\pi (1 - \eta) k_l (k_l^2 - (2\pi f)^2)}{(k_l^2 + (2\pi f)^2)^2}, \end{aligned} \quad (13)$$

III. PHEROMONE PROPAGATION AND CHANNEL MODELING

After the release of VOCs from the leaf, they start to propagate in the medium. Depending upon the environment, the medium can be water for aquatic plants and air for terrestrial plants. However, in this section, we will consider air as the propagating medium and describe the VOC propagation depending on the VOC emission type.

To begin with, we initialize the modeling with some assumptions. We consider a constant wind velocity (u) in the medium. The wind flow is classified according to Pasquill-Gifford (PG) into 6 stability classes: A (strongly unstable), B (moderately unstable), C (slightly unstable), D (neutral), E (slightly stable), and F (moderately stable) [24]. However, the D stability class is observed during both the daytime and nighttime. Hence, we will consider class D as our wind stability, whose velocity typically varies from 3-7 m/s [24].

The VOCs emitted from the leaf start to propagate through the medium. That propagation of VOCs is governed by Fick's law of diffusion, which is well documented in the literature [20], [25], [26], given by:

$$\frac{\partial c(\vec{r}, t)}{\partial t} + \nabla \cdot \vec{J}(\vec{r}, t) = S(\vec{r}, t), \quad (14)$$

where $c(\vec{r}, t)$ is the concentration at a position $\vec{r} \in \mathbb{R}^3$, ∇ is the Laplace operator in 3-D Cartesian coordinates, $\vec{J}(\vec{r}, t)$ is the flux of VOCs at position \vec{r} , and $S(\vec{r}, t)$ is the source term.

The flux of VOCs ($\vec{J}(\vec{r}, t)$) depends on both the advection due to the wind and diffusion caused by the turbulence in the atmosphere, expressed as:

$$\vec{J}(\vec{r}, t) = \vec{J}_A(\vec{r}, t) + \vec{J}_D(\vec{r}, t), \quad (15)$$

Considering \vec{u} as the wind velocity, the advection-diffusion can be expressed as:

$$\vec{J}_A(\vec{r}, t) = c(\vec{r}, t) \vec{u}, \quad (16)$$

Furthermore, due to the turbulent wind flow, eddy diffusion (K) is encountered by the VOCs. The flux can be expressed by Fick's law of motion:

$$\vec{J}_D(\vec{r}, t) = -K \nabla c(\vec{r}, t), \quad (17)$$

By substituting (15-17) in (14), the obtained expression is as follows:

$$\frac{\partial c(\vec{r}, t)}{\partial t} + \nabla \cdot (c(\vec{r}, t) \vec{u}) - \nabla \cdot (K \nabla c(\vec{r}, t)) = S(\vec{r}, t), \quad (18)$$

(18) needs to be solved in order to obtain the closed-form solution considering suitable initial and boundary conditions. However, it is important to note that the solution of the PDE may not always exist. In order to solve the PDE, we will consider some assumptions based on the type of VOC emission.

After the release, the propagation of the VOCs depends on the medium and also the type of release. According to the release type, the propagation can be modeled via Gaussian Models. The use of Gaussian models in air-based propagation is well documented [27]–[29]. For the stress-driven VOC release, we consider the Gaussian Puff model, as it deals with the sudden release of a fixed amount of VOCs.

A. Channel Modeling for Stress-driven VOC Emission

We consider some assumptions in order to model the puff concentration profile, where the wind velocity is constant and also directed in the x -axis ($u, 0, 0$). According to Taylor's theory, the dispersion coefficients are used to describe the effects of eddy diffusion in atmospheric transport modeling [30]. In realistic atmospheric conditions, the diffusion is anisotropic and depends upon the downwind distance x . The governing equation for the puff model is expressed as [31]:

$$c(\vec{r}, t) = \frac{Q_0}{(2\pi)^{\frac{3}{2}} \sigma_x \sigma_y \sigma_z} e^{-\frac{1}{2} \left(\frac{x-x_0-u t}{\sigma_x} \right)^2} e^{-\frac{1}{2} \left(\frac{y-y_0}{\sigma_y} \right)^2} \left[e^{-\frac{(z-z_0)^2}{2\sigma_z^2}} + e^{-\frac{(z+z_0)^2}{2\sigma_z^2}} \right], \quad (19)$$

where $c(\vec{r}, t)$ is the spatiotemporal concentration, Q_0 is the number of released VOCs, σ_x , σ_y , σ_z are the dispersion coefficients in x , y , and z direction, respectively. x_0 , y_0 , z_0 are the 3D coordinate of the VOC release point. Furthermore, we consider that VOCs are released from a certain height z_0 , i.e., $(0, 0, z_0)$. The longitudinal diffusion is negligible compared to advection and is often omitted in the Gaussian puff models [16]. However, this does not imply the absence of dispersion along the x -direction. In reality, turbulent eddies induce a finite and small longitudinal spread. To capture this behavior, we approximate the longitudinal dispersion as the geometric mean of lateral and vertical spreads, i.e.,

$$\sigma_x = \sqrt{\sigma_y \sigma_z}, \quad (20)$$

Hence, (19) reduces to:

$$c(\vec{r}, t) = \frac{Q_0}{(2\pi \sigma_y \sigma_z)^{\frac{3}{2}}} e^{-\frac{1}{2} \left(\frac{x-u t}{\sqrt{\sigma_y \sigma_z}} \right)^2} e^{-\frac{1}{2} \left(\frac{y}{\sigma_y} \right)^2} \left[e^{-\frac{(z-z_0)^2}{2\sigma_z^2}} + e^{-\frac{(z+z_0)^2}{2\sigma_z^2}} \right], \quad (21)$$

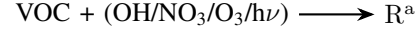
The dispersion coefficient depends on the turbulent airflow and the stability class. There are multiple ways to determine these coefficients, like Briggs [32], Briggs dispersion coefficients that are revised by Griffiths [33], as shown in Table I, and

TABLE I
PUFF DISPERSION COEFFICIENT FORMULAS [31]

PG stability class	σ_y (m)	σ_z (m)
A	$0.18x^{0.92}$	$0.60x^{0.75}$
B	$0.14x^{0.92}$	$0.53x^{0.73}$
C	$0.10x^{0.92}$	$0.34x^{0.71}$
D	$0.06x^{0.92}$	$0.15x^{0.70}$
E	$0.04x^{0.92}$	$0.10x^{0.65}$
F	$0.02x^{0.89}$	$0.05x^{0.61}$

computational methods like genetic algorithm and particle swarm optimization [34].

However, during the propagation, VOCs are influenced by two modalities: chemical interference and air turbulence [35]. The Gaussian models inherently consider the air turbulence via the dispersion coefficients [36]. Hence, we need to consider the chemical interference of VOCs. Initially, depending on the type of VOCs, they react with OH radicals, NO_3 radicals, and O_3 atoms or undergo photodissociation in the troposphere and form alkyl or substituted alkyl radicals (R^a) (e.g., hydroxylalkyl, nitrooxyalkyl or oxoalkyl). Furthermore, those R^a 's undergoes a sequential reaction to produce a stable product [37]. The equation can be expressed as:



As soon as R^a 's are produced in the troposphere, the properties of VOCs are lost, and those are no longer considered as the information carrier in the interplant communication process. Since byproducts do not participate in interplant signaling, subsequent reactions are beyond the scope of the communication channel model. The rate of the reaction (R) can be given as follows:

$$R = k[\text{VOC}][\text{oxidant}], \quad (22)$$

where k is the second-order rate constant, and $[\text{VOC}]$ and $[\text{oxidant}]$ are the concentration of VOC and oxidants ($\text{OH}/\text{NO}_3/\text{O}_3$), respectively. Replacing the VOC concentration at \vec{r} in (22), the rate of the reaction becomes:

$$R = k_{eff} c(\vec{r}, t), \quad (23)$$

where $k_{eff} = \sum_i k_i [\text{oxidant}]_i$. Considering this VOC degradation, a partial differential equation (PDE) can be expressed as:

$$\frac{dc}{dt} = -k_{eff} t, \quad (24)$$

The solution of (24) is given by:

$$c_d(\vec{r}, t) = c(\vec{r}, t) e^{-k_{eff} t}, \quad (25)$$

Hence, the concentration profile considering the VOC degradation is expressed as:

$$c_d(\vec{r}, t) = \frac{Q_0}{(2\pi \sigma_y \sigma_z)^{\frac{3}{2}}} e^{-\frac{1}{2} \left(\frac{x-u t}{\sqrt{\sigma_y \sigma_z}} \right)^2} e^{-\frac{1}{2} \left(\frac{y}{\sigma_y} \right)^2} e^{-k_{eff} t} \left[e^{-\frac{(z-z_0)^2}{2\sigma_z^2}} + e^{-\frac{(z+z_0)^2}{2\sigma_z^2}} \right], \quad (26)$$

Fourier transform of (26) is given by:

$$H_{sc}(f) = \frac{Q_0}{2\pi u \sigma_y \sigma_z} e^{-\frac{y^2}{2\sigma_y^2}} \left[e^{-\frac{(z-z_0)^2}{2\sigma_z^2}} + e^{-\frac{(z+z_0)^2}{2\sigma_z^2}} \right] e^{(k_{eff} - i2\pi f) \frac{x}{u}} \cdot e^{(k_{eff} - i2\pi f)^2 \frac{\sigma_y \sigma_z}{u^2}}, \quad (27)$$

Gain can be expressed as:

$$H_{sc}^g(f) = \frac{Q_0}{2\pi u \sigma_y \sigma_z} e^{-\frac{y^2}{2\sigma_y^2}} \left[e^{-\frac{(z-z_0)^2}{2\sigma_z^2}} + e^{-\frac{(z+z_0)^2}{2\sigma_z^2}} \right] \cdot e^{k_{eff} \frac{x}{u} + (k_{eff}^2 - (2\pi f)^2) \frac{\sigma_y \sigma_z}{u^2}}, \quad (28)$$

The normalized gain is given by:

$$H_{sc}^n(f) = \frac{|H_{sc}^g(f)|}{\max_f |H_{sc}^g(f)|}, \quad (29)$$

The phase can be expressed as:

$$\phi_{sc}(f) = -2\pi f \frac{x}{u} - 4\pi f k_{eff} \frac{\sigma_y \sigma_z}{u^2}, \quad (30)$$

Hence, the delay will be:

$$\tau_{sc}(f) = 2\pi \frac{x}{u} + 4\pi k_{eff} \frac{\sigma_y \sigma_z}{u^2}, \quad (31)$$

B. Channel Modeling for Constitutive VOC Emission

The constitutive VOC emission is evident to be released continuously [8], and the continuous VOC emission can be modeled by the Gaussian plume model. The Gaussian plume is considered as a borderline case of puffs and the combination of multiple puffs that are close to each other [38]. Hence, the concentration profile of the plume can be expressed as:

$$c_p(\vec{r}) = \int_0^\infty c_d(\vec{r}, t) dt, \quad (32)$$

where $c_d(\vec{r}, t)$ is the concentration profile of the Gaussian Puff model considering VOC degradation in the atmosphere, which is modeled in (26). Solving (32), the obtained concentration profile is:

$$c_p(\vec{r}) = \frac{Q_0}{2\pi u \sigma_y \sigma_z} e^{-\frac{y^2}{2\sigma_y^2}} \left[e^{-\frac{(z-z_0)^2}{2\sigma_z^2}} + e^{-\frac{(z+z_0)^2}{2\sigma_z^2}} \right] e^{-k_{eff} \frac{x}{u}}, \quad (33)$$

In order to find the normalized gain, we need to obtain the Fourier transform of (33), and given by:

$$H_{ccs}(f) = c_p(\vec{r}) \cdot \delta(f), \quad (34)$$

As seen in (34), the Fourier transform is only defined at $f = 0$. Even though the continuous VOC release is considered, the amount of VOC changes due to environmental factors like circadian rhythm and weekly or seasonal variation. Hence, we intend to model the channel to capture this effect by considering VOC variation in a 24-hour window. Hence, $\Delta t = 86400$ s. According to the time-frequency uncertainty principle [39],

$$\Delta t \cdot \Delta f \geq \frac{1}{4\pi}, \quad (35)$$

Hence, $\Delta f \geq 9.21 \times 10^{-6}$ Hz. With this consideration, (34) becomes:

$$H_{cc}(f) = c_p(\vec{r}) \cdot G(f), \quad (36)$$

where $G(f)$ is the Gaussian approximated delta function and expressed as:

$$G(f) = \frac{1}{\sqrt{2\pi} \Delta f} e^{-\frac{f^2}{2\Delta f^2}}, \quad (37)$$

The normalized gain is given by:

$$H_{cc}^n(f) = \frac{|H_{cc}(f)|}{\max |H_{cc}(f)|}, \quad (38)$$

(36) does not explicitly contain any phase term and, therefore, doesn't produce any delay. This is because the plume model considers that VOCs have been emitted continuously for an infinite time, and the system is in a quasi-steady state at the time of observation. However, the absence of the delay term doesn't imply instantaneous transport of VOCs. It can be explained as the receiver is continuously exposed to a VOC concentration that integrates the cumulative effects of past emissions. It is important to note that even though the continuous emission doesn't yield a delay, the delay is implicitly encoded in the derivation from the time-dependent Gaussian puff model, which is explained in Sec. III-A. For this reason, the delay is considered to be zero for continuous emission, not due to the physical absence of propagation time but due to the quasi-steady nature of the model.

C. Noise Model

In ICT, noise is any signal other than the signal of interest that influences a receiver. Like other communication techniques, VOC communication is also prone to noise, especially when we discuss long-range VOC communication. We usually discuss this on the basis of a single plant being used as a transmitter and another plant as a receiver. However, in the environment, multiple plant species are available, and their response to biotic/abiotic stresses widely differ [40]. Hence, while inter-plant communication occurs within two plants, other nearby plants, which are exposed to similar or any other kind of stress, would also release VOCs as a response. Under constitutive emission, VOCs are released continuously by the transmitter plant, which results in a continuous circadian rhythm following concentration profile. While there is a finite delay due to transport mechanisms, the receiver plant may continuously sense VOC presence and potentially infer transmitter state or identity information, even in noisy environments. However, as stress-driven VOC release is instantaneous, it is highly influenced by the VOCs of different plant species, which is not the point of interest in the model; hence, it is considered as noise.

The trade-off between the signal and the noise depends on the induced stress, the type of plant species, the ratio/number of the sources, and the distance among them. The signal-to-noise ratio (SNR) can expressed as:

$$SNR = \frac{P_0}{P_N}, \quad (39)$$

where P_0 is the average power of the signal, and P_N is the average power of noise. Considering the same height of the noise release point, SNR becomes:

$$SNR = \frac{\frac{1}{n} \sum_{t=0}^{n-1} Q_0^2 \cdot e^{-\frac{(x-ut)^2}{\sigma_y \sigma_z}} e^{-\frac{y^2}{\sigma_y^2}} e^{-2k_{eff}t}}{\frac{1}{n} \sum_{t=0}^{n-1} Q_N^2 \cdot e^{-\frac{(x-x_0-ut)^2}{\sigma_y \sigma_z}} e^{-\frac{(y-y_0)^2}{\sigma_y^2}} e^{-2k_N t}}, \quad (40)$$

where Q_N is the number of noise VOC released, k_N is the effective rate constant of noise. (40) depicts the SNR for a single signal and power source. However, this equation can be modified according to the number of signal and noise sources, which is as follows:

$$SNR_{mn} = \frac{\sum_{m=1}^k P_0}{\sum_{n=1}^l P_S}, \quad (41)$$

where SNR_{mn} is the SNR for multiple signal and noise sources, and m and n depict the number of signal and noise sources, respectively.

IV. RECEPTION MODEL

There are several mathematical models that exist for the description of the reception process, namely linear regression model [41], partition model [42], and mechanistic ordinary differential equation (ODE) based model [43]. However, a comparative study of these models shows that the ODE-based model best resembles the experimental data [44]. Hence, we consider the ODE-based approach in this study to explore the reception process.

The mass balance approach is followed to determine the deposition of molecules on the leaf. The rate of change in concentration in the leaf is given by [43], [44]:

$$\frac{dC_R(t)}{dt} = -lC_R(t) + b, \quad (42)$$

where $C_R(t)$ is the concentration of molecules in the leaf, l is the loss term, and b is the uptake term. The loss term α depends on the surface area of a leaf (A_l), conductance (G_l), leaf volume (V_l), leaf-air partition coefficient (K_{LA}), and a pseudo-first-order rate constant for plant growth (P_{growth}) in the following way:

$$l = K_{LA} \frac{A_l G_l}{V_l} + P_{growth}, \quad (43)$$

The uptake term (b) is given as:

$$b = \frac{A_l G_l}{V_l} c(\vec{r}, t), \quad (44)$$

where $c(\vec{r}, t)$ is the gas phase concentration in the air. The Fourier transform of (42) can be given as:

$$C_r(f) = \frac{b}{j2\pi f + l} c(\vec{r}, f), \quad (45)$$

Hence, the transfer function is given by:

$$H_r(f) = \frac{b}{j2\pi f + l}, \quad (46)$$

The normalized gain is expressed as:

$$H_r^n(f) = \frac{l}{\sqrt{4\pi^2 f^2 + l^2}}, \quad (47)$$

TABLE II
PHYSICOCHEMICAL PARAMETERS FOR VARIOUS VOC COMPOUNDS IN *Q. Ilex* [21], [45].

Compound	k_a (s ⁻¹)	k_l (×10 ⁻⁵ s ⁻¹)	k_d (s ⁻¹)	η
α -Pinene	0.002459	3.37791	0.7	0.867
β -Pinene	0.002455	5.31881	0.9	0.846
Myrcene	0.001565	15.281	3	0.840
Sabinene	0.002953	0.4044	2.5	0.629
cis- β -Ocimene	0.001167	4.1857	1.5	0.782
p-Cymene	0.000844	0.7434	2	0.697
γ -Terpinene	0.001395	2.4189	1.7	0.811
α -Terpinolene	0.001126	1.1959	1.3	0.736
β -Phellandrene	0.001319	0.5852	2.3	0.762

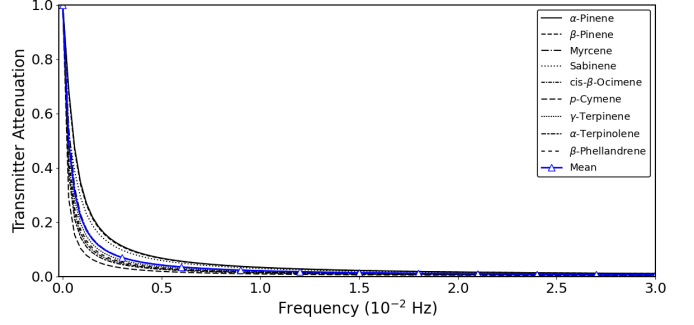


Fig. 3: Attenuation of transmission process over frequency.

and the phase is given by:

$$\phi_r(f) = \tan^{-1} \frac{2\pi f}{l}, \quad (48)$$

Hence, delay is expressed as:

$$\tau_r(f) = \frac{2\pi}{l(1 + (2\pi f/l)^2)}, \quad (49)$$

V. RESULTS AND DISCUSSIONS

In Sec. II, III, and IV, the transmission, channel, and reception processes of interplant VOC communication are modeled. In this section, a detailed analysis of the communication architecture is described. In order to understand the transmitter characteristics from a molecular communication perspective, we consider *Quercus ilex* (*Q. ilex*) as the transmitter plant. The monoterpenoid emission is considered as the signal for transmission, and the characteristic parameters are given in Table II.

Firstly, the attenuation of the transmission process is illustrated in Fig. 3. The release of blended monoterpenoids from the leaves constitutes several VOCs, and it can be seen that the attenuation drops sharply over frequency. Even though stress-driven VOC emission is modeled as an instantaneous burst, which corresponds to a broad frequency spectrum, due to biological constraints like VOC transport through cuticle and chemical partitioning, higher frequencies are highly attenuated. This results in an effective bandwidth of less than 0.002 Hz, which resembles a narrowband, Gaussian-approximated delta function. Fig. 4 depicts the delay of the transmission process over the frequency. Similar to the attenuation, they delay profile of different VOCs also decreases with frequency. In *Q. ilex*, α -pinene is the most abundant monoterpenoid, and

TABLE III
VOC COMPOSITIONS IN Q. ILEX AND PINUS PINEA.

Compound	Composition in Q. ilex (%) [45]	Composition in Pinus pinea (%) [46]
α -Pinene	32.0718	0.4341
β -Pinene	24.6972	0.0894
Myrcene	12.9217	1.3788
Sabinene	10.5861	0.4979
cis- β -Ocimene	5.1687	1.3660
p-Cymene	4.3577	—
γ -Terpinene	4.2604	—
α -Terpinolene	3.2115	—
β -Phellandrene	2.7249	—
Acetone	—	12.3057
Limonene	—	1.2384
trans- β -Ocimene	—	70.7136
Linalool	—	6.4343

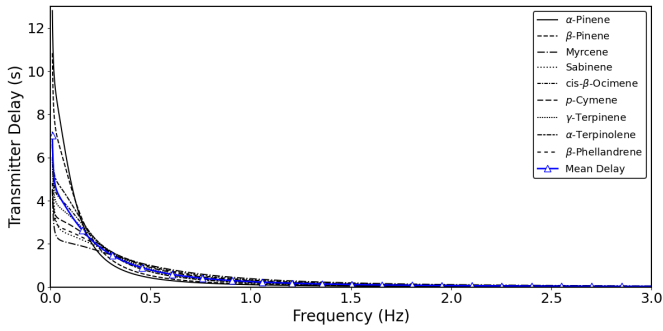


Fig. 4: Delay of transmission process with respect to frequency.

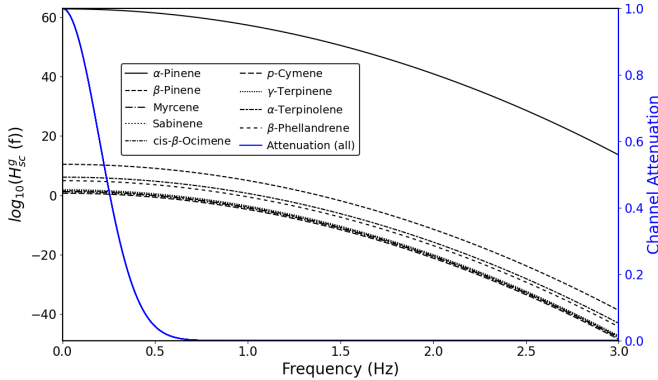


Fig. 5: $\log_{10}(H_{sc}^g(f))$ and attenuation of the channel over frequency at a distance of 100 meters with a velocity of 7 m/s.

its delay is maximum initially, which is 12.8 sec, though the delay doesn't depend upon the number of released molecules. The mean delay of the released VOCs is 7.02 sec and falls rapidly with frequency. The observed sharp decrease in delay suggests that leaf cells allow fast pheromone movements, which enables signal propagation for high frequencies with zero delay.

The interplant channel characteristics for stress-driven or instantaneous VOC release are modeled in Sec. III-A and are analyzed here. For the propagation of blended VOCs in the channel, a total of Q_0 molecules is considered. The number of individual VOC released by Q. Ilex is followed according to the ratio of the total emission pool, which is given in Table III. The rate constants that are required to determine k_{eff} are given

TABLE IV
ARRHENIUS RATE CONSTANT (k (CM³ MOLECULE⁻¹ S⁻¹)) AT ROOM TEMPERATUR.

VOC compound	OH ($\times 10^{-12}$)	NO ₃ ($\times 10^{-11}$)	O ₃ ($\times 10^{-17}$)	Ref.
α -pinene	52.3	84	6.16	[37]
β pinene	74.3	15	2.51	[37]
Myrcene	215	1.1	47	[37]
Sabinene	117	1.0	8.3	[37]
cis- β -Ocimene	252	2.2	54	[37]
p-Cymene	151	0.99	0.2	[47], [48]
γ -Terpinene	177	2.9	14	[37]
α -Terpinolene	225	9.7	190	[37]
β -Phellandrene	168	8	4.7	[37]
Acetone	0.17	2.9×10^{-6}	0.9×10^{-4}	[37]
Limonene	164	1.22	21	[37]
trans- β -Ocimene	252	2.2	54	[37]
Linalool	159	1.12	43	[49]

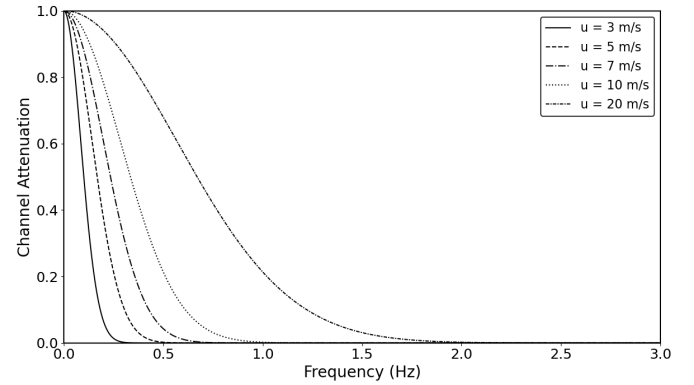


Fig. 6: Channel attenuation w.r.t frequency for different velocities at a distance of 100 meter.

in Table IV. Moreover, the concentration of OH, O₃, and NO₃ are 2×10^6 , 7×10^{11} , and 1×10^{10} molecules/cm³, respectively, and the number of released VOCs (Q_0) is 10000. Fig. 5 depicts the channel behavior both in terms of gain and attenuation at a distance of 100 meters with a velocity of 7 m/s. It can be observed that the gain, plotted as $\log_{10}(H_{sc}^g(f))$, widely varies according to the type of VOC and decreases gradually with the frequency. This variation arises due to the differences in the kinetic parameters of different VOCs. However, the attenuation for the channel is identical across all VOCs, which rapidly drops as the frequency increases. It confirms that individual VOCs may behave differently due to molecular properties, but the medium imposes a common high-frequency attenuation, which significantly limits the effective bandwidth and behaves like a low-pass filter.

Fig. 6 depicts the effect of wind velocity variation on the channel attenuation over frequency at a fixed distance of 100 meters. The channel exhibits low-pass behavior for all velocities, with higher attenuation at increasing frequencies. It is noticeable that as the wind velocity increases, the attenuation shifts toward higher frequencies. This means that higher velocities result in broader bandwidths, and high-frequency components of the VOC signal can propagate more effectively. This trend can be explained by the fact that increasing the wind speed reduces the presence time of VOCs in the medium, which decreases the effect of reactive decay and dispersion.

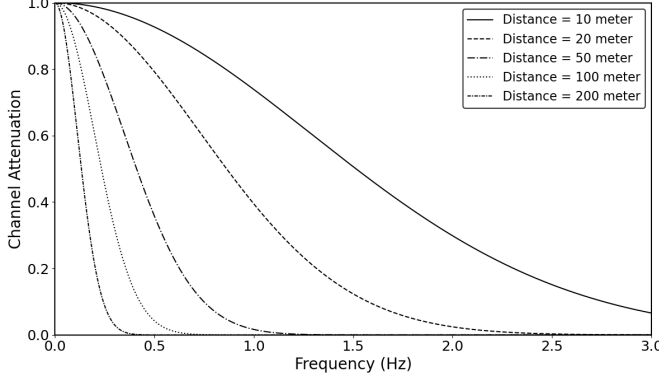


Fig. 7: Channel attenuation w.r.t frequency at different distances at a velocity of 7 m/s.

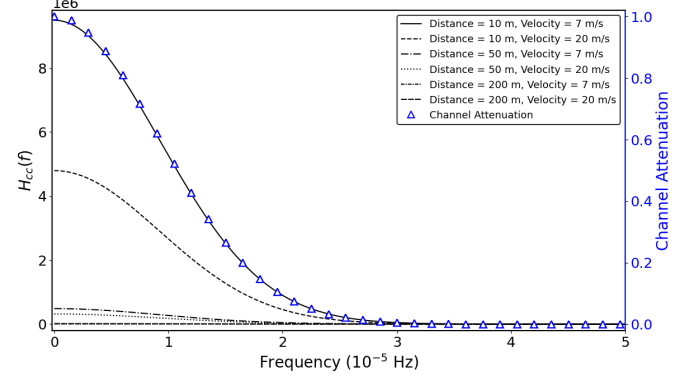


Fig. 9: $H_{cc}^n(f)$ and channel attenuation w.r.t frequency at different distances and velocities for constitutive VOC emission.

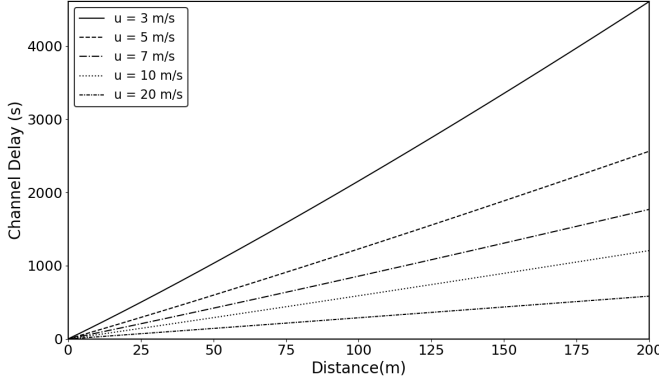


Fig. 8: Delay of channel with respect to distance at different velocities.

Hence, the attenuation pattern confirms that the wind speed plays a crucial role in shaping the frequency response of the VOC-based MC channel.

Fig. 7 depicts the variation of channel attenuation over frequency for different transmission distances with a fixed wind velocity of 7 m/s. It illustrates that as the distance increases, the attenuation accelerates, which leads to a reduced effective bandwidth for greater distances. At shorter distances (e.g., 10 or 20 meters), the attenuation is gradual, allowing a broader spectrum of frequency components to pass through. The physical interpretation of this behavior is due to the enhanced molecular degradation and dispersion over longer distances; VOCs undergo more interactions with atmospheric reactants and experience greater spread, which weakens the signal strength at higher frequencies. This figure explains that transmission distance is a limiting factor for interplant VOC communication and must be considered while designing a bio-inspired MC system.

Fig. 8 illustrates the variation of channel delay with respect to distance for different wind velocities. The graph shows a linear relationship between delay and distance, which indicates that the channel introduces uniform propagation delay across distances. It is also observed that the higher velocities lead to significantly lower delays at the same distance. For instance, at 200 meters, the delay is 4609 seconds for 3 m/s but drops to 584 seconds for 20 m/s. This behavior can be explained

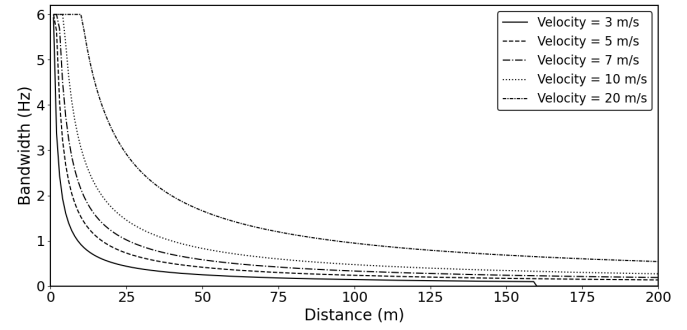


Fig. 10: Bandwidth of the channel w.r.t distance at different velocities.

by the fact that faster wind helps VOCs to propagate more quickly, reducing the time required to reach the receiver plant. The separation between the curves also increases with distance, which emphasizes the impact of wind speed over longer ranges. Hence, for faster and more reliable VOC-based information transfer, higher velocities, short distances, or both are favorable.

Moreover, constitutive VOC release, which is modeled in Sec. III-B is described hereafter. Fig. 9 illustrates the gain $H_{cc}(f)$ and channel attenuation with respect to frequency for various combinations of propagation distance and wind velocity for continuous VOC release conditions. It is observed that the channel exhibits a strong low-pass behavior, where the gain sharply declines with increasing frequency. The plot shows that shorter distances and lower velocities yield higher gain w.r.t frequency. This is because slower wind speeds allow VOCs to remain concentrated in the channel for a longer period, which minimizes molecular spread and degradation. The normalized attenuation (shown by the blue triangular curve) falls off rapidly, implying that the channel can only support very low-frequency components, which are typically under 2×10^{-5} Hz. This suggests that high-frequency VOC modulation is not sustainable, and only very slowly varying biochemical signals can reliably propagate, which is indeed the physicality of the constitutive VOC release mechanism of plants for MC. Fig. 10 elucidates the variation of channel bandwidth with respect to distance for different wind velocities. It is observed that the effective bandwidth decreases

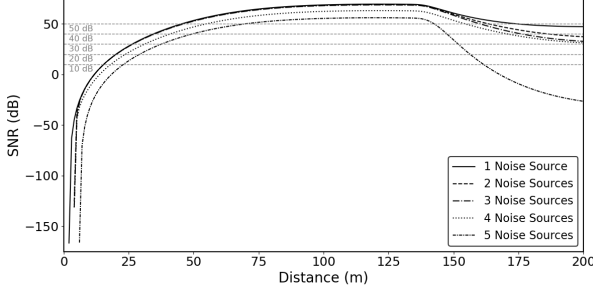


Fig. 11: SNR w.r.t distance considering 5 nearby noise sources at 7 m/s.

sharply with increasing distance. For shorter distances and higher velocities, the bandwidth remains significantly high due to low dispersion and VOC degradation.

Furthermore, the noise analysis that is modeled in III-C is analyzed from the ICT perspective. Fig. 11 depicts the SNR as a function of distance at a velocity of 7 m/s under the influence of the increasing number of nearby noise sources up to five. It is notable that the SNR is highly influenced by the position of the noise and the number of noise sources. In total, five noises are considered, and their positions are (2,1), (2,-1), (4,2), (4,-2), and (6,0). The noise sources are analyzed as a cumulative source, i.e., by considering a single noise source, then two noise sources are considered, and so on, up to a total of 5 noise sources together. *Pinus pinea* is considered as a noise source; due to different leaf architecture and species, the emission of this widely differed from the *Q. ilex*, as mentioned in Table III. With this step-up, the SNR initially increases, reflecting the accumulation of signal as it travels through the medium. However, beyond approximately 140 meters, SNR begins to decline or flatten depending on the noise configuration. This behavior arises as the VOC signal is modeled as a Gaussian pulse centered at $x = u \cdot t$, which has a finite window, considering $t \in [0, 20]$ seconds and $u = 7$ m/s. For this reason, if the signal front reaches $x \approx 140$ m, the signal energy starts to decay, but the noise continues to contribute to the background concentration. The variation between SNR curves is due to different noise sources either constructively or destructively interfering with the signal. This result highlights the importance of considering the spatiotemporal structure of signal propagation for long-distance VOC communication. With the noise analysis, it is observed that the VOC communication architecture can be used for different purposes depending on the interplant distance. The SNR below 10 dB indicates that the signal is hard to distinguish from noise and is not suitable for any kind of communication. SNR between 10 and 20 dB is of poor quality, but SNR from 20 to 30 dB is considered in low-speed communication. 30 to 40 dB SNR is used in voice communication and cell phones. Finally, SNR above 40 dB is considered to be of excellent quality and is used in digital signals and high-speed communication systems. Consequently, based on the SNR determined by the spatial configuration of the signal and noise sources, VOC-based MC communication can link the nano-network with micro-scale devices, which can be merged with traditional communication through the internet in the micro-device.

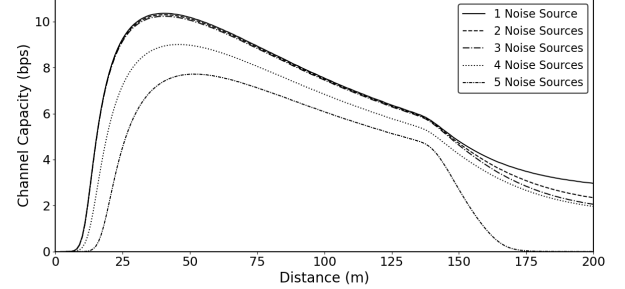


Fig. 12: Channel capacity w.r.t distance at 7 m/s considering 5 nearby noise sources.

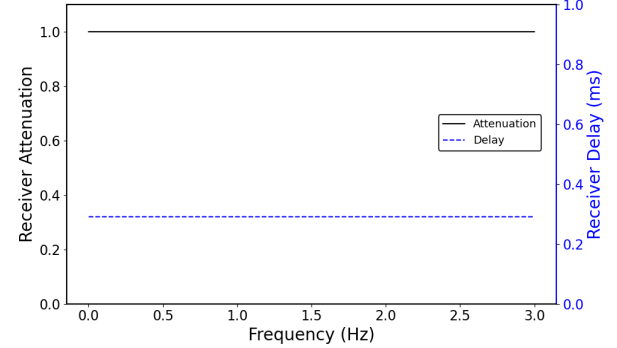


Fig. 13: Attenuation and delay of receiver over frequency.

Fig. 12 illustrates the corresponding channel capacity calculated using the Shannon formula, incorporating both the bandwidth data from Fig. 10 and the SNR profile from Fig. 11. The Shannon capacity (C) formula is expressed as:

$$C = B \cdot \log_2(1 + SNR), \quad (50)$$

where B is the bandwidth and C is expressed in bits per second (bps). It is observed that the capacity initially increases with distance, reaching a peak before gradually declining. This can be explained by a trade-off between the initially increasing bandwidth at short ranges and the declining SNR at longer distances. At higher distances, both bandwidth and SNR decrease, resulting in a capacity drop. Furthermore, increasing noise levels considerably lowers the overall channel capacity. These results collectively indicate that the MC physical channel layer in the interplant communication system is highly sensitive to propagation distance, flow conditions, and background noise. Optimization of these parameters is required to ensure high-throughput and reliable information transfer in interplant communication networks.

Fig. 13 shows the attenuation and delay of the receiver as a function of frequency by considering $A_l = 5 \text{ m}^2$, $G_l = 86.4 \text{ m/day}$, $V_l = 0.002 \text{ m}^3$, $K_{LA} = 10$, $P_{growth} = 0.035 \text{ /day}$ [44], [50]. The attenuation of the receiver remains constant at ~ 1 , and the delay stays flat at ~ 0.3 ms. This indicates that the plant receiver exhibits a frequency-independent response without a noticeable distortion, which resembles a linear and memoryless communication channel.

Furthermore, an end-to-end channel model can be done by modeling end-to-end channel attenuation ($H_e(f)$) with the obtained normalized gain in (7), (29), and (47) via $H_e(f) =$

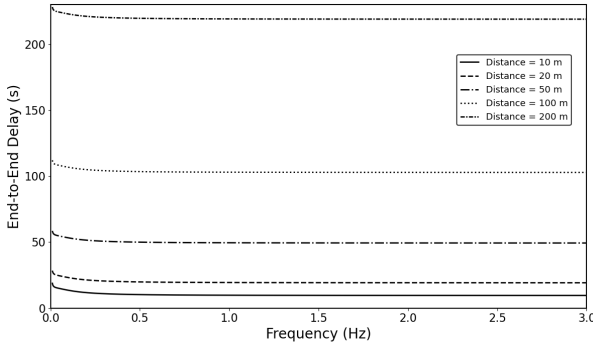


Fig. 14: End-to-end channel delay over frequency at different transmitter-receiver distance.

$H_{Tx}^n(f) \cdot H_{sc}^n(f) \cdot H_r^n(f)$. It can be inferred from Fig. 3, 6, and 13 that the end-to-end channel attenuation is dominated by the transmitter attenuation as the attenuation rapidly drops to zero at ~ 10 mHz, which implies that the end-to-end channel has a very narrow bandwidth. Hence, it can only support very slow varying or low-frequency signaling. Although the end-to-end channel is limited by the transmitter's characteristics, the physical channel exhibits a broader bandwidth, implying that the physical channel is capable of transmitting faster variations in VOC concentration.

Moreover, the delay of the end-to-end channel can be given by $\tau_e(f) = \tau_{Tx}(f) + \tau_{sc}(f) + \tau_r(f)$. Fig. 14 depicts the delay of the end-to-end channel at a constant wind velocity of 7 m/s for multiple transmitter-receiver distances. It can be observed that the delay is dominated by the physical channel delay. The delay increases with increasing distance due to the longer time required for VOCs to drift through the channel, which is dominant over VOC diffusion in the physical channel.

VI. CONCLUSION

In this paper, the VOC-based interplant MC channel is studied from the ICT perspective. It is comprised of three stages: transmission, physical channel, and reception. In the transmission process, leaves produce VOCs and store them in aqueous and lipid pools; from there, those VOCs diffuse to the intracellular air space and are released into the ambient air. In the physical channel, these VOCs travel considering the advection-diffusion mechanism in the turbulent wind flow condition, where they undergo VOC degradation due to the presence of oxidants. The propagation of the VOCs can be modeled in different ways according to the emission type; for the stress-induced VOC emission, the Gaussian puff model is preferred, whereas the Gaussian plume model is used for constitutive VOC emission. Lastly, when these VOCs reach to the receiver plant, the VOCs are uptaken by the leaves, and physiological signaling pathways are created according to the received VOC concentration or the ratio in the blended VOC. All these stages are discussed according to the attenuation and delay of VOCs. This study demonstrates that VOC-based interplant MC is highly distance and velocity-sensitive, exhibiting low-pass characteristics and narrow bandwidths. While the physical channel supports moderately higher frequencies, the transmitter's biological constraints greatly limit

the end-to-end capacity, which makes the system suitable only for slow-varying VOC signals. The potential for long-range communication in VOC-based MC, along with the natural abundance of VOCs in intra- and interspecies signaling, makes this paradigm highly suitable for designing reliable, bio-inspired communication architectures that interface nanonetworks with microscale systems.

REFERENCES

- [1] N. Farsad, H. B. Yilmaz, A. Eckford, C.-B. Chae, and W. Guo, "A comprehensive survey of recent advancements in molecular communication," *IEEE Communications Surveys & Tutorials*, vol. 18, no. 3, pp. 1887–1919, 2016.
- [2] I. F. Akyildiz, F. Brunetti, and C. Blázquez, "Nanonetworks: A new communication paradigm," *Computer Networks*, vol. 52, no. 12, pp. 2260–2279, 2008.
- [3] M. Kuscu, E. Dinc, B. A. Bilgin, H. Ramezani, and O. B. Akan, "Transmitter and receiver architectures for molecular communications: A survey on physical design with modulation, coding, and detection techniques," *Proceedings of the IEEE*, vol. 107, no. 7, pp. 1302–1341, 2019.
- [4] N. Dudareva, A. Klempien, J. K. Muhlemann, and I. Kaplan, "Biosynthesis, function and metabolic engineering of plant volatile organic compounds," *New Phytologist*, vol. 198, no. 1, pp. 16–32, 2013.
- [5] V. Ninkovic, D. Markovic, and M. Rensing, "Plant volatiles as cues and signals in plant communication," *Plant, cell & environment*, vol. 44, no. 4, pp. 1030–1043, 2021.
- [6] R. Grote, R. K. Monson, and Ü. Niinemets, "Leaf-level models of constitutive and stress-driven volatile organic compound emissions," in *Biology, controls and models of tree volatile organic compound emissions*. Springer, 2013, pp. 315–355.
- [7] N. Dudareva, F. Negre, D. A. Nagegowda, and I. Orlova, "Plant volatiles: recent advances and future perspectives," *Critical reviews in plant sciences*, vol. 25, no. 5, pp. 417–440, 2006.
- [8] F. Loreto and S. D'Auria, "How do plants sense volatiles sent by other plants?" *Trends in plant science*, vol. 27, no. 1, pp. 29–38, 2022.
- [9] M. Ameye, S. Allmann, J. Verwaeren, G. Smagghe, G. Haesaert, R. C. Schuurink, and K. Audenaert, "Green leaf volatile production by plants: a meta-analysis," *New Phytologist*, vol. 220, no. 3, pp. 666–683, 2018.
- [10] V. Ninkovic, D. Markovic, and I. Dahlin, "Decoding neighbour volatiles in preparation for future competition and implications for tritrophic interactions," *Perspectives in Plant Ecology, Evolution and Systematics*, vol. 23, pp. 11–17, 2016.
- [11] Y. Dong, J. Li, W. Zhang, H. Bai, H. Li, and L. Shi, "Exogenous application of methyl jasmonate affects the emissions of volatile compounds in lavender (*Lavandula angustifolia*)," *Plant Physiology and Biochemistry*, vol. 185, pp. 25–34, 2022.
- [12] J. K. Holopainen and J. Gershenzon, "Multiple stress factors and the emission of plant VOCs," *Trends in plant science*, vol. 15, no. 3, pp. 176–184, 2010.
- [13] R. N. Kigathi, W. W. Weisser, M. Reichelt, J. Gershenzon, and S. B. Unsicker, "Plant volatile emission depends on the species composition of the neighboring plant community," *BMC plant biology*, vol. 19, pp. 1–17, 2019.
- [14] R. Wheatley, "The consequences of volatile organic compound mediated bacterial and fungal interactions," *Antonie Van Leeuwenhoek*, vol. 81, pp. 357–364, 2002.
- [15] S. Fischer, P. Trefz, A. Bergmann, M. Steffens, M. Ziller, W. Miekisch, J. S. Schubert, H. Köhler, and P. Reinhold, "Physiological variability in volatile organic compounds (VOCs) in exhaled breath and released from faeces due to nutrition and somatic growth in a standardized caprine animal model," *Journal of breath research*, vol. 9, no. 2, p. 027108, 2015.
- [16] B. D. Unluturk and I. F. Akyildiz, "An end-to-end model of plant pheromone channel for long range molecular communication," *IEEE transactions on nanobioscience*, vol. 16, no. 1, pp. 11–20, 2016.
- [17] T.-M. Koski, T. Laaksonen, E. Mäntylä, S. Ruuskanen, T. Li, P. S. Girón-Calva, L. Huttunen, J. D. Blande, J. K. Holopainen, and T. Klemlola, "Do insectivorous birds use volatile organic compounds from plants as olfactory foraging cues? Three experimental tests," *Ethology*, vol. 121, no. 12, pp. 1131–1144, 2015.
- [18] Ü. Niinemets, A. Kännaste, and L. Copolovici, "Quantitative patterns between plant volatile emissions induced by biotic stresses and the degree of damage," *Frontiers in Plant Science*, vol. 4, p. 262, 2013.

[19] M. S. Waring and J. R. Wells, "Volatile organic compound conversion by ozone, hydroxyl radicals, and nitrate radicals in residential indoor air: Magnitudes and impacts of oxidant sources," *Atmospheric Environment*, vol. 106, pp. 382–391, 2015.

[20] L. P. Giné and I. F. Akyildiz, "Molecular communication options for long range nanonetworks," *Computer Networks*, vol. 53, no. 16, pp. 2753–2766, 2009.

[21] P. C. Harley, "The roles of stomatal conductance and compound volatility in controlling the emission of volatile organic compounds from leaves," in *Biology, controls and models of tree volatile organic compound emissions*. Springer, 2013, pp. 181–208.

[22] A. Fahn, "Structure and function of secretory cells," in *Advances in Botanical Research*, ser. Advances in Botanical Research. Academic Press, 2000, vol. 31, pp. 37–75.

[23] P. S. Nobel, "Chapter 1 - cells and diffusion," in *Physicochemical and Environmental Plant Physiology (Fourth Edition)*, fourth edition ed., P. S. Nobel, Ed. San Diego: Academic Press, 2009, pp. 2–43.

[24] D. Turner, *Workbook of Atmospheric Dispersion Estimates: An Introduction to Dispersion Modeling*, 2nd ed. CRC Press, 1994.

[25] M. Pierobon and I. F. Akyildiz, "A physical end-to-end model for molecular communication in nanonetworks," *IEEE Journal on Selected Areas in Communications*, vol. 28, no. 4, pp. 602–611, 2010.

[26] A. Powari and O. B. Akan, "Odor Intensity Shift Keying (OISK) and Channel Capacity of Odor-Based Molecular Communications in Internet of Everything," *IEEE Transactions on Molecular, Biological, and Multi-Scale Communications*, 2024.

[27] N. Lotrecchiano, D. Sofia, A. Giuliano, D. Barletta, M. Poletto *et al.*, "Pollution dispersion from a fire using a Gaussian plume model," *Int. J. Saf. Secur. Eng.*, vol. 10, pp. 431–439, 2020.

[28] N. K. Arystanbekova, "Application of Gaussian plume models for air pollution simulation at instantaneous emissions," *Mathematics and Computers in Simulation*, vol. 67, no. 4–5, pp. 451–458, 2004.

[29] P. De Haan and M. W. Rotach, "A novel approach to atmospheric dispersion modelling: The Puff-Particle Model," *Quarterly Journal of the Royal Meteorological Society*, vol. 124, no. 552, pp. 2771–2792, 1998.

[30] G. I. Taylor, "Diffusion by continuous movements," *Proceedings of the london mathematical society*, vol. 2, no. 1, pp. 196–212, 1922.

[31] H. Li, J. Zhang, and J. Yi, "Computational source term estimation of the Gaussian puff dispersion," *Soft Computing*, vol. 23, pp. 59–75, 2019.

[32] G. Briggs, "Diffusion estimation for small emission," *Environmental Res. Lab, Air Resource Atmos. Turb. & Diff. Lab*, 1973.

[33] R. Griffiths, "Errors in the use of the Briggs parameterization for atmospheric dispersion coefficients," *Atmospheric Environment*, vol. 28, no. 17, pp. 2861–2865, 1994.

[34] L. M. Q. Abualigah and E. S. Hanandeh, "Applying genetic algorithms to information retrieval using vector space model," *International Journal of Computer Science, Engineering and Applications (IJCSEA) Vol*, vol. 5, 2015.

[35] J. K. Wilson, A. Kessler, and H. A. Woods, "Noisy communication via airborne infochemicals," *BioScience*, vol. 65, no. 7, pp. 667–677, 2015.

[36] X. Cao, G. Roy, W. J. Hurley, and W. S. Andrews, "Dispersion coefficients for Gaussian puff models," *Boundary-layer meteorology*, vol. 139, pp. 487–500, 2011.

[37] R. Atkinson and J. Arey, "Atmospheric degradation of volatile organic compounds," *Chemical reviews*, vol. 103, no. 12, pp. 4605–4638, 2003.

[38] H. Snoun, M. Krichen, and H. Chérif, "A comprehensive review of Gaussian atmospheric dispersion models: current usage and future perspectives," *Euro-Mediterranean Journal for Environmental Integration*, vol. 8, no. 1, pp. 219–242, 2023.

[39] J. N. Oppenheim and M. O. Magnasco, "Human time-frequency acuity beats the Fourier uncertainty principle," *Physical review letters*, vol. 110, no. 4, p. 044301, 2013.

[40] J. Kesselmeier, K. Bode, U. Hofmann, H. Müller, L. Schäfer, A. Wolf, P. Ciccioli, E. Brancaleoni, A. Cecinato, M. Frattoni *et al.*, "Emission of short chained organic acids, aldehydes and monoterpenes from *Quercus ilex* L. and *Pinus pinea* L. in relation to physiological activities, carbon budget and emission algorithms," *Atmospheric Environment*, vol. 31, pp. 119–133, 1997.

[41] E. Bacci, D. Calamari, C. Gaggi, and M. Vighi, "Bioconcentration of organic chemical vapors in plant leaves: experimental measurements and correlation," *Environmental science & technology*, vol. 24, no. 6, pp. 885–889, 1990.

[42] M. Riederer, "Estimating partitioning and transport of organic chemicals in the foliage/atmosphere system: discussion of a fugacity-based model," *Environmental science & technology*, vol. 24, no. 6, pp. 829–837, 1990.

[43] S. Trapp and M. Mathies, "Generic one-compartment model for uptake of organic chemicals by foliar vegetation," *Environmental science & technology*, vol. 29, no. 9, pp. 2333–2338, 1995.

[44] C. D. Collins and E. Finnegan, "Modeling the plant uptake of organic chemicals, including the soil- air- plant pathway," *Environmental science & technology*, vol. 44, no. 3, pp. 998–1003, 2010.

[45] Ü. Niinemets and M. Reichstein, "A model analysis of the effects of nonspecific monoterpenoid storage in leaf tissues on emission kinetics and composition in Mediterranean sclerophyllous *Quercus* species," *Global Biogeochemical Cycles*, vol. 16, no. 4, pp. 57–1, 2002.

[46] S. M. Noe, P. Ciccioli, E. Brancaleoni, F. Loreto, and Ü. Niinemets, "Emissions of monoterpenes linalool and ocimene respond differently to environmental changes due to differences in physico-chemical characteristics," *Atmospheric Environment*, vol. 40, no. 25, pp. 4649–4662, 2006.

[47] S. B. Corchnoy and R. Atkinson, "Kinetics of the gas-phase reactions of hydroxyl and nitrogen oxide (NO₃) radicals with 2-carene, 1, 8-cineole, p-cymene, and terpinolene," *Environmental science & technology*, vol. 24, no. 10, pp. 1497–1502, 1990.

[48] R. Atkinson, D. Hasegawa, and S. M. Aschmann, "Rate constants for the gas-phase reactions of O₃ with a series of monoterpenes and related compounds at 296±2 K," *International Journal of Chemical Kinetics*, vol. 22, no. 8, pp. 871–887, 1990.

[49] R. Atkinson, J. Arey, S. M. Aschmann, S. B. Corchnoy, and Y. Shu, "Rate constants for the gas-phase reactions of cis-3-Hexen-1-ol, cis-3-Hexenylacetate, trans-2-Hexenal, and Linalool with OH and NO₃ radicals and O₃ at 296±2 K, and OH radical formation yields from the O₃ reactions," *International Journal of Chemical Kinetics*, vol. 27, no. 10, pp. 941–955, 1995.

[50] E. Terzaghi, R. Posada-Baquero, A. Di Guardo, and J.-J. Ortega-Calvo, "Microbial degradation of pyrene in holm oak (*Quercus ilex*) phyllosphere: Role of particulate matter in regulating bioaccessibility," *Science of the Total Environment*, vol. 786, p. 147431, 2021.



Bitop Maitra (Graduate Student Member, IEEE) received his B.Tech degree in Electronics and Communication Engineering from the University of Calcutta, Kolkata, India, in 2019 and the M.Tech in Biomedical Engineering from the National Institute of Technology, Rourkela, India, in 2021. He is pursuing his Ph.D. in Electrical and Electronics Engineering from Koç University and is a research assistant at the Center for neXt-generation Communications (CXC). His research interests lie in abiogenesis, molecular communication, and related areas.



Ozgur B. Akan (Fellow, IEEE) received his Ph.D degree from the Georgia Institute of Technology, Atlanta, GA, USA, in 2004. He is currently the Head of the Internet of Everything (IoE) Group with the Department of Engineering, University of Cambridge, UK, and the Director of the Centre for neXt-generation Communications (CXC), Koç University, Turkey. His research interests include wireless, nano, and molecular communications and the Internet of Everything.